

**Emissions of Methane-methane from Coalcoal, Thermal-thermal power plants and Wetlands-wetlands and its implications on Atmospheric-atmospheric Methane-methane across the South Asian region**

Mahalakshmi D.Venkata<sup>1</sup>., Mahesh Pathakoti<sup>1\*</sup>, Asuri-Lakshmi Kanchana<sup>1</sup>, Sujatha Peethani<sup>2</sup>,  
Ibrahim Shaik<sup>1</sup>, Krishnan Sundara Rajan<sup>3</sup>, Vijay Kumar Sagar<sup>4</sup>, Pushapanathan Raja<sup>5</sup>,  
Yogesh K.Tiwari<sup>4</sup>, Prakash Chauhan<sup>1</sup>

<sup>1</sup>National Remote Sensing Centre (NRSC), Indian Space Research Organisation (ISRO), Hyderabad, India-500037

<sup>2</sup>Formerly at The International Center for Agricultural Research in the Dry Areas

<sup>3</sup>Lab for Spatial Informatics, International Institute of Information Technology (IIIT), Hyderabad-5000084, India

<sup>4</sup>Indian Institute of Tropical Meteorology (IITM), Pune, India-411008.

<sup>5</sup>ICAR-Indian Institute of Soil and Water Conservation, Research Centre, Koraput, Odisha, India-763 002.

\*Corresponding author: mahi952@gmail.com

**Abstract**

Atmospheric methane (CH<sub>4</sub>) is a potent climate change agent responsible for a fraction of global warming. The present study investigated the spatio-temporal variability of atmospheric column-averaged (X) CH<sub>4</sub> (XCH<sub>4</sub>) concentrations using Greenhouse gases Observing SATellite (GOSAT) and TROPOspheric Monitoring Instrument onboard the Sentinel -5 Precursor (S5P/TROPOMI) data from 2009 to 2022 over the South Asia region. During the study period, the long-term trends in XCH<sub>4</sub> increased from 1700 ppb to 1950 ppb with an annual growth rate of 8.76 ppb year<sup>-1</sup>. Among all natural and anthropogenic sources of CH<sub>4</sub>, the rate of increase in XCH<sub>4</sub> was higher over the coal site at about 10.15 ppb year<sup>-1</sup> (Paschim Bardhaman) followed by Mundra ultra mega power plant at about 9.72 ppb year<sup>-1</sup>. The majority of the wetlands exhibit an annual trend of XCH<sub>4</sub> more than 9.50 ppb year<sup>-1</sup> with a minimum rate of 8.72 ppb year<sup>-1</sup> over Wular Lake. The WetCHARTs-based emissions of CH<sub>4</sub> from the wetlands were minimal during the winter and pre-monsoon seasons. Maximum CH<sub>4</sub> flux was observed during the monsoon with a maximum value of 23.62±3.66 mg m<sup>-2</sup> month<sup>-1</sup> over the Sundarbans wetland. For the 15 Indian Agroclimatic zones, significant high emissions of CH<sub>4</sub> were observed over the Middle Gangetic Plains (MGP), Trans Gangetic Plains (TGP), Upper Gangetic Plains (UGP), East Coast Plains & Hills (ECPH), Lower Gangetic Plains (LGP) and East Gangetic Plains (EGP). Further, the bottom-up anthropogenic CH<sub>4</sub> emissions data are mapped against the XCH<sub>4</sub> concentrations and a high correlation was found in the Indo Gangetic Plains (IGP) region, indicating the hotspots of anthropogenic CH<sub>4</sub>. The present study highlighted the impact of natural and anthropogenic sources of XCH<sub>4</sub> and quantified the spatio-temporal changes in XCH<sub>4</sub> at each study site over the Indian region.

**Keywords:** GOSAT, S5P/TROPOMI, Column-averaged CH<sub>4</sub>, South Asia, spatio-temporal, anthropogenic emissions.

## 1. Introduction

Atmospheric methane ( $\text{CH}_4$ ) is one of the high-potential greenhouse gases (GHG) ~~and that plays an vital role in the chemistry of the atmosphere. regulates the chemical reactions in the free troposphere and stratosphere.~~ In the troposphere,  $\text{CH}_4$  oxidation is due to hydroxyl (OH) radical (OH) and produces results in the production of carbon monoxide, carbon dioxide,  $\text{CO}_2$  and ozone in the presence of increased amounts of oxides of nitrogen. In contrast, ~~where as in the stratosphere, oxidation of  $\text{CH}_4$  is by OH radical, atomic oxygen and chlorine (Nair and Kavitha, 2020). Through oxidation by the OH radical 90% of  $\text{CH}_4$  in the atmosphere breaks down. Atmospheric composition, humidity, UV radiation and temperature are the vital parameters which determine the abundance of hydroxyl radical (Skeie et al., 2023).~~  $\text{CH}_4$  has enormous potential for global warming, about 28–36 times that of  $\text{CO}_2$  over 100 years (IPCC, 2021), and a comparatively short perturbation lifespan of about 12 years (Balcombe et al., 2018). Over the past decade, the research community has become more interested in anthropogenic  $\text{CH}_4$  concentration due to its persistent rise in the atmosphere, and lack of knowledge regarding its source or sink (Huang et al., 2015). The long-term  $\text{CH}_4$  observations from the National Oceanic and Atmospheric Administration (NOAA) have shown a yearly increase of 8 ppb  $\text{CH}_4$  year<sup>-1</sup>, while Shadnagar, an Indian site, shows an increase of 10 ppb year<sup>-1</sup> (Sreenivas et al., 2022). Though the emissions have increased over the past 20 years, the causes ~~remain are still unclear not clearly understood.~~ Recent research suggests that a combination of fossil fuel and agricultural emissions, with fluctuations in the  $\text{CH}_4$  sink in the atmosphere, also plays a part (Schaefer et al., 2016; Worden et al., 2017; Turner et al., 2019; Zhang et al., 2022). The decadal budget indicates that relative uncertainties may range from 20 to 35 % for inventories of anthropogenic emissions in specific sectors (food waste, agriculture, and fossil fuels), 50 to 100 % for emissions from burning biomass and emissions from natural wetland ecosystems, and 100% or more for emissions from other natural sources. Geographically, India's wetlands ~~comprise make up~~ 4.7% of the nation's total land area (Bassi et al., 2014; Kavitha et al., 2016). The primary sources of  $\text{CH}_4$  emissions include natural emissions from freshwater systems, wetlands, and geological sources; anthropogenic emissions come from waste management, agriculture, and the mining and burning of fossil fuels (Kirschke et al., 2013; Saunio et al., 2016a; Ganesan et al., 2019).

Wetlands are the natural sources that contribute to 20–40% of global emissions and dominate the inter-annual variability (Parker et al., 2018). Only limited studies have been ~~conducted carried out~~ in India about  $\text{CH}_4$  discharge ~~of methane~~ from wetlands. A recent study (Vinna et al., 2021) shows that natural wetlands could produce 50% to 80% more  $\text{CH}_4$  emissions by 2100. According to Schlesinger et al. (2009), wetlands, rice paddies, and ruminants are the leading producers of  $\text{CH}_4$  on the Indian subcontinent. According to Hayashida et al. (2013), there is a seasonal pattern in the  $\text{CH}_4$  concentration over the Indian subcontinent, with higher values during the post-monsoon and minimum in pre-monsoon. Kavitha et al., (2016) used the Scanning Imaging Absorption spectrometer for Atmospheric Cartography (SCIAMACHY) retrieved ~~data to~~ retrieve methane product over the Indian region to understand the spatio-temporal variations.

The salient findings of this study are that during monsoon and post-monsoon, -high XCH<sub>4</sub> values are observed in the Northern regions. Different seasonal behaviour is observed with seasonal peak in post-monsoon and low during monsoon in the Southern peninsular regions. These regional variations are ~~to~~-due to the distribution of sources like livestock population, rice cultivation, wetland, biomass burning and oil and gas mining. Along with temperature, precipitation, and radiation, the CH<sub>4</sub> emissions from the natural wetlands might affect the region's heat budgeting, exacerbating global warming on a local, regional, and even ~~on~~-global scale (Sakalli et al., 2017). Thermal power plants are responsible for a large amount of the GHG emissions from the energy sector. Each thermal power plant has a different set of emission factors for methane and nitrous oxide, ~~which are~~-based on operating conditions and combustion technology (Kang et al., 2019). The integrated measure of CH<sub>4</sub> includes contributions from the various vertical atmospheric layers, ranging from the Earth's surface measurement point to the uppermost layer of the atmosphere. Chandra et al. (2017) studied the raised air mass ~~into~~ the 600–200 hPa height layer over northern India, which accounts for 40% of the seasonal CH<sub>4</sub> augmentation during the southwest monsoon season. Conversely, in the semi-arid region, the height over 600 hPa contributed up to approximately 88% of the amplitude of the XCH<sub>4</sub> seasonal cycle, while the atmosphere below 600 hPa contributed only around 12%. The feature of air mass transport processes in the Asian monsoon region is the main reason for the increased contributions from above 600 hPa across the northern Indian region.

Insufficient datasets exist regardingabout the CH<sub>4</sub> feedback originating from wetlands; a study on the precise estimation of CH<sub>4</sub> outflow from wetlands and its impact ~~inon~~ local/regional global warming scenarios is ~~therefore~~-urgently needed. The ability to identify spatial and temporal fluctuations in atmospheric CH<sub>4</sub> from space, due to recent technological developments in remote sensing, could help fill in the gaps left by measurements performed by ships, planes, and the ground (Frankenberg et al., 2008; Kuze et al., 2009; [Kavitha et al., 2018](#)). The present study focuses on the Implications of emissions from ~~C~~coal, ~~T~~thermal power plants, and ~~W~~wetlands on atmospheric methane over ~~S~~south ~~Asia~~asia using XCH<sub>4</sub> data from Greenhouse gases Observing SATellite (GOSAT) and TROPOspheric Monitoring Instrument onboard the Sentinel-5 Precursor (S5P/TROPOMI) from 2009 to 2022. It has further analyzed the spatial and temporal pattern of atmospheric CH<sub>4</sub>-variations and emissions and its correlation with anthropogenic CH<sub>4</sub> emissions from the bottom-up emission inventory of the Emission Database for Global Atmospheric Research (EDGAR).The wetland methane emissions were addressed using WetCHARTs v1.3.1S over the top 10 wetland sites -inof the present study. -The response of atmospheric CH<sub>4</sub> concentrations to anthropogenic emissions in various agroclimatic zones of India was further highlighted in this study using the XCH<sub>4</sub> data from 2001 to 2022.

## 2. Study region

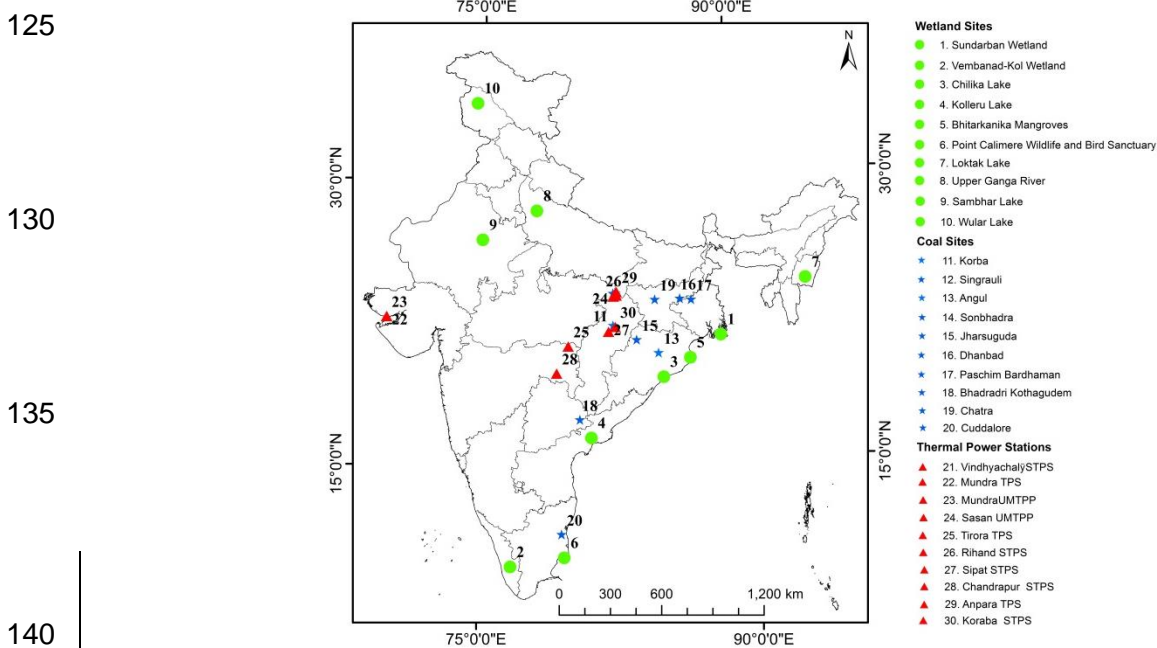


Figure 1 study locations a) top 10 coal mine locations in India based on production capacity indicated by star (★); b) top 10 thermal power stations denoted by triangle (▲) and c) top 10 wetlands selected based on the area represented by circle (●).

The distribution of heterogeneous sources of CH<sub>4</sub> sources over the Indian region are is shown in Figure 1. The focus of the study was Tthree heterogenic—CH<sub>4</sub> source regions—coal fields, thermal power plants, and the Ramsar Wwetlands were the focus of the present study. The number of coal mines in India varies from 1 to 65, and the top ten coal fields were selected for this study based on their production capacity. During 2019–2020, coal and lignite production was between 0.1 and 120.47 MT. The study's coal mine details are provided in Table 1.-2. Similarly, Table 23 lists thermal power stations according to their respective power generation. The Ramsar Convention is an international agreement created in 1971 to protect wetlands and promote their sustainable use (<https://rsis Ramsar.org>). The Ministry of Environment, Forests and Climate Change (MoEF&CC), Government of India, has identified 75 Ramsar Wetland sites in India as of November 2022. These sites span a total area of 13,35,530 ha. Based on the high total geographical area coverage (Table 3-4), the top 10 places were determined for the current investigation. The size varies from 423000 ha (Sundarbans wWetland, West Bengal) to 18900 ha (Wular Lake, Jammu and Kashmir) (https://indianwetlands.in/wetlands-overview/indias-wetlands-of-international-importance/; PIB Press Release on World Wetlands Day dated 26<sup>th</sup> August, 2022).

### 3. Data and Methodology

The GOSAT series developed by the Japan Aerospace Exploration Agency (JAXA) continuously monitors ~~provides For continuous monitoring of~~ CO<sub>2</sub> and CH<sub>4</sub> from space (Kuze et al., 2009). The present study obtained, the level 2 (L2) column CH<sub>4</sub> (XCH<sub>4</sub>) from the GOSAT ~~data obtained from the Greenhouse gases Observing SATellite (GOSAT) series developed by the Japan Aerospace Exploration Agency (JAXA) (Kuze et al., 2009)~~. Onboard the GOSAT, the Thermal and Near Infrared (NIR) Sensor for Carbon Observation Fourier-Transform Spectrometer (TANSO-FTS) is used to detect the CO<sub>2</sub> and CH<sub>4</sub> absorption spectra in the shortwave IR (1.60µm & 2.0µm) region (Kuze et al., 2009; Kavitha et al., 2018). Ground-based FTIR measurements of XCH<sub>4</sub> by the Total Carbon Column Observing Network (TCCON) are used extensively to validate the GOSAT retrievals. Retrieval bias and precision of column abundance from GOSAT SWIR observations have been estimated as approximately 15-20 ppb and 1%, respectively (Morino et al., 2011; Yoshida et al., 2013). In the present study, the atmospheric CH<sub>4</sub> was obtained from 2009 to 2022 within a 100 km radius of the coal mines. The data corresponding to the quality flag (=0) was considered for the study only.

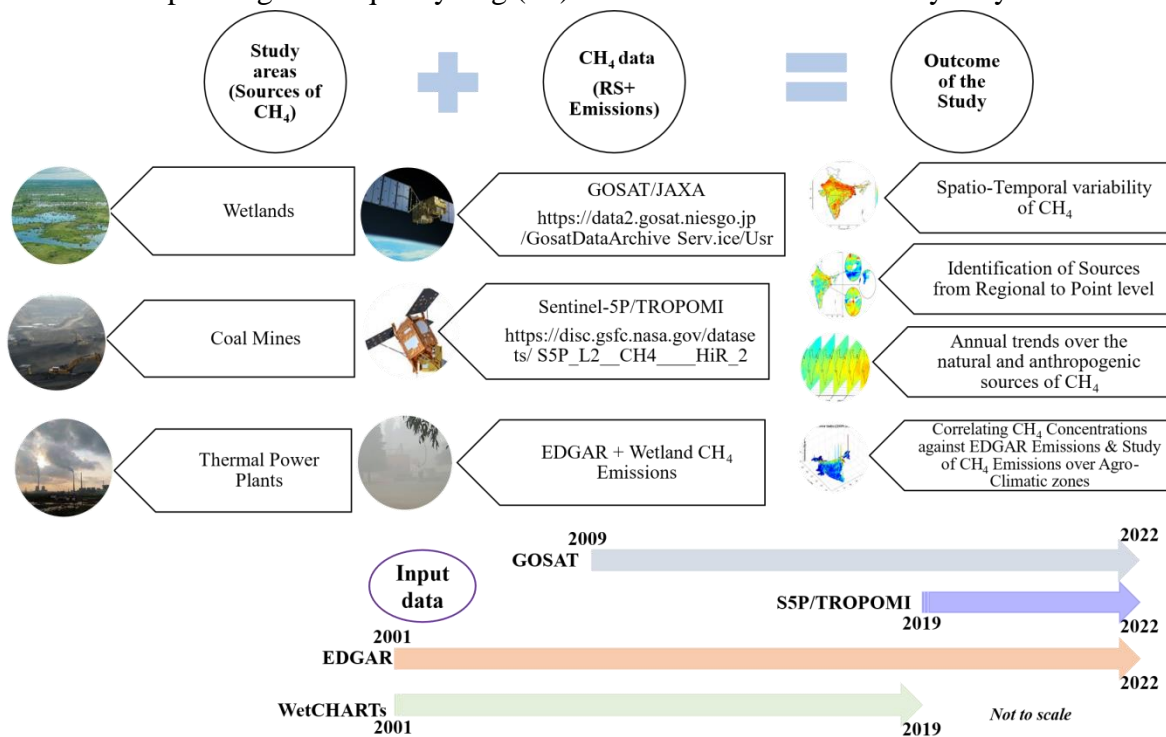


Figure 2 Data resources and ~~S~~study approach

The Sentinel-5 Precursor satellite, ~~which was~~ launched on October 13, 2017, is equipped with the TROPospheric Monitoring Instrument (TROPOMI), which tracks cloud characteristics, aerosols, and trace gases (Sentinel-5p. 2019). With a daily pass time of approximately 13:30 local solar time, the instrument's spectrometer measures reflected sunlight in the ultraviolet,

185 | visible, NIRnear-IR, and SWIR spectral windows. The CH<sub>4</sub> retrieval algorithm uses the two  
spectral bands, i.e., reflectance in NIR (757-774 nm) and SWIR (2305-2385 nm) (Kozicka et al.,  
2023). Initially, retrievals based on TROPOMI had a high-spatial resolution of 7 km x 3.5 km  
(along-track x across-track, Bergamaschi et al., 2022). From August 2019 to the present, the  
190 | resolution has been increased to 5.5 km × 3.5 km (Sagar et al., 2022). The latest data version is  
now v2 from 2021-07-01 to now. The quality flag (<0.5) was only considered as per the product  
readme file document (Sentinel-5p. 2019). Methane retrieval from TROPOMI ~~agrees in overall~~  
~~agreement with correlative~~ with ground based FTIR XCH<sub>4</sub> retrievals from TCCON and the  
Network for Detection of Atmospheric Composition Change (NDACC). The systematic  
differences of the bias-corrected XCH<sub>4</sub> data with respect to TCCON ~~data~~ and NDACC data are,  
195 | on average, -0.26±0.56% and 0.57±0.83%, respectively (Song et al., 2023). The data within the  
coal mines and wetlands area are taken from 01<sup>st</sup> May 2018 to 30<sup>th</sup> April, 2022. The individual  
shape files were given for each wetland field, and the satellite passes within the area were  
considered for the current study. As shown in Figure 2, a detailed procedure is explained in this  
section. The present study utilized the total anthropogenic emissions from the EDGAR  
200 | (<https://edgar.jrc.ec.europa.eu/gallery?release=v50&substance=CH4&sector=TOTALS>, accessed  
on 01<sup>st</sup> November 2023) respectively. Uncertainties in the information on source intensity,  
activity and other statistical data are the key parameters for the uncertainties in the EDGAR  
emission inventory (Janardanan et al., 2017). Bottom-up inventory uncertainties range between  
205 | 20 and 35% for agriculture, waste and fossil fuel sectors; 50% for biomass burning and natural  
wetland emissions and 100% or higher for natural sources such as geological seeps and inland  
waters for global methane emissions (Saunio et al., 2020). Further, the present study also  
utilized wetland methane emissions (mg m<sup>-2</sup>month<sup>-1</sup>) from WetCHARTs v1.3.1  
([https://daac.ornl.gov/CMS/guides/MonthlyWetland\\_CH4\\_WetCHARTs.html](https://daac.ornl.gov/CMS/guides/MonthlyWetland_CH4_WetCHARTs.html)) which is  
available at spatial resolution of 0.5°×0.5° with monthly temporal resolution and scale factor  
210 | utilized here is 124.5 TgCH<sub>4</sub>yr<sup>-1</sup>. We have selected the coal fields based on the production as  
shown in Table 1. The data on all coal mines in India, their production, and their location are  
accessed from the  
<https://dataverse.harvard.edu/dataset.xhtml?persistentId=doi:10.7910/DVN/TDEK80>. Each  
district has open cast or underground types of mines found in India, and the number of coal  
215 | mines varies from 1 to 65. The coal/Lignite production was 0.1 to 120.47 MT during 2019-  
2020. The details of the coal mines in the present study are summarized in Table 1, and locations  
are mapped in Figure 1.

220

S.No	District names	No. of Mines	Production (MT)	Latitude	Longitude
1	Korba	15	120.47	22.47	82.56
2	Singrauli	7	82.19	24.15	82.6
3	Angul	13	80.61	20.97	85.11
4	Sonbhadra	5	47.36	24.15	82.74
5	Jharsuguda	9	36.71	21.69	83.89
6	Dhanbad	51	31.25	23.76	86.46
7	Paschim Bardhaman	65	31.23	23.68	87.11
8	Bhadradi Kothagudem	14	30.16	17.57	80.58
9	Chatra	4	29.65	23.76	85.01
10	Cuddalore	3	23.46	11.55	79.5

Table 1. The district names, the total number of coal mines, total production, and their centroid (latitudes and longitudes) locations of mines in the respective districts. ~~in 2019-2020.~~

225

The list is prepared based on the descending order of total production in each district in India. There are 262 thermal power stations with a full capacity of 229.335 Gigawatt (GW) and a total unit of 2689 in India, based on diesel, gas turbine, and steam as on March 31, 2020. Table 2 shows the list of thermal power stations.

230

S.No	Power Stations names	Installed Capacity (MW)	No. of Units	Latitude (N)	Longitude (E)
1	Vindhyachal STPS	4760	13	24.1	82.68
2	Mundra TPS	4620	9	22.82	69.55
3	Mundra UMTTP	4000	5	22.82	69.53
4	Sasan UMTTP	3960	6	23.98	82.62
5	Tirora TPS	3300	5	21.41	79.97
6	Rihand STPS	3000	6	24.03	82.79
7	Sipat STPS	2980	5	22.14	82.29
8	Chandrapur STPS	2920	7	20	79.3
9	Anpara TPS	2630	7	24.21	82.8
10	Korba STPS	2600	7	22.39	82.68

Table 2. Top 10 thermal power plants based on their capacity.

235 | There are 11 [new](#) Ramsar sites identified in 2022 (total 75 sites) by the Ministry of Environment Forests and Climate Change (MoEF&CC), India, covering a total area of 1,093,636 ha 2022. The present study considered the top 10 sites based on the high area coverage (Table 3) for the current study. The area ranges from 18900 ha (Wular Lake) to 423000 ha (Sundarban Wetland).

240

S.No	Wetlands Location	Latitude (N)	Longitude (E)	Area (ha)
1	Sundarban Wetland	21.77	88.71	423000
2	Vembanad-Kol Wetland	9.83	76.75	151250
3	Chilika Lake	19.7	85.35	116500
4	Kolleru Lake	16.61	81.2	90100
5	Bhitarkanika Mangroves	20.65	86.9	65000
6	Point Calimere Wildlife and Bird Sanctuary	10.31	79.63	38500
7	Loktak Lake	24.43	93.81	26600
8	Upper Ganga River	28.55	78.2	26590
9	Sambhar Lake	27	75	24000
10	Wular Lake	34.26	74.55	18900

Table 3. Top 10 Wetlands fields based on their area coverage.

245

250

255

260



## 4. Results and Discussion

### 4.1. Spatio-temporal variability of Space-based Atmospheric CH<sub>4</sub>

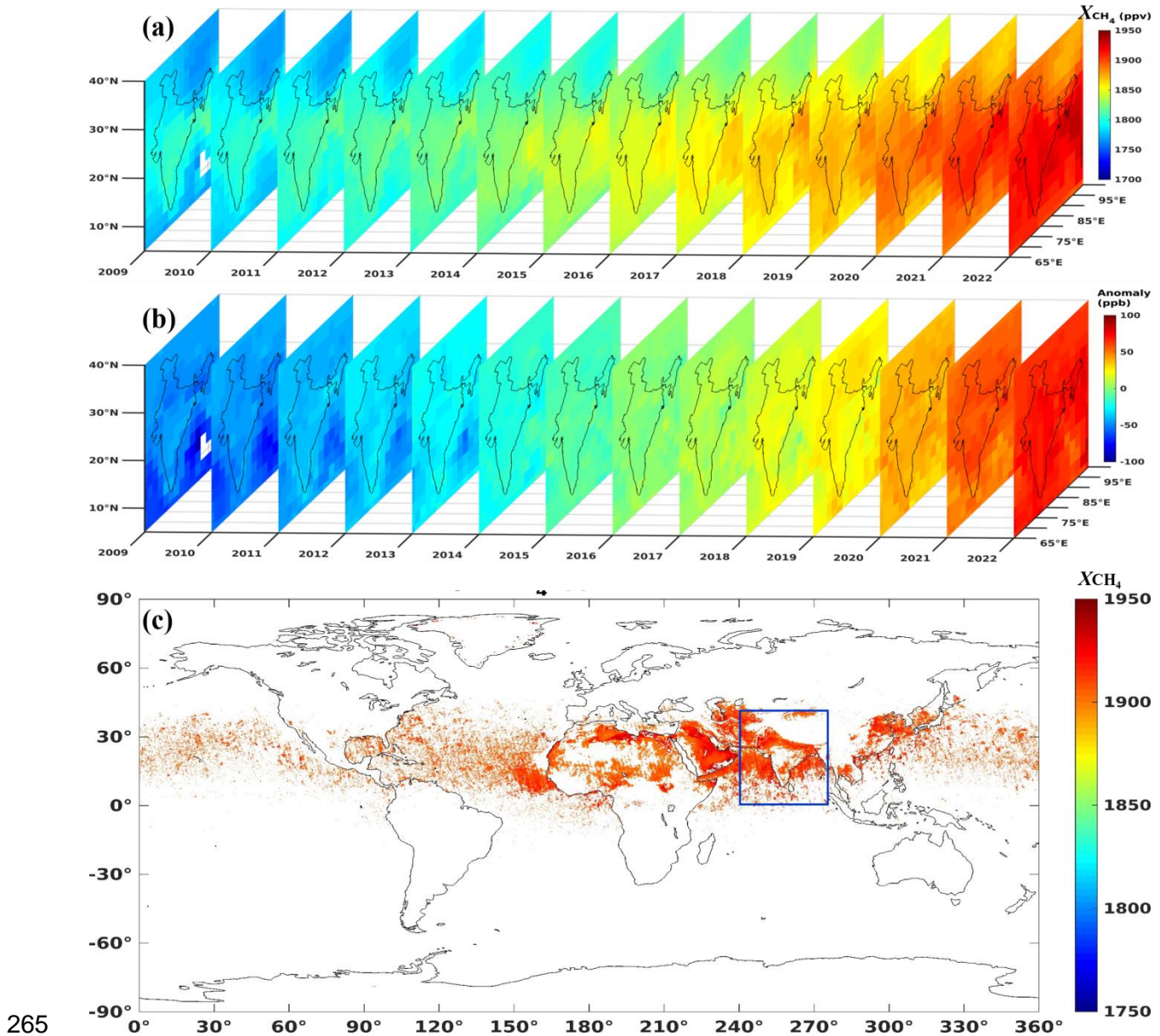


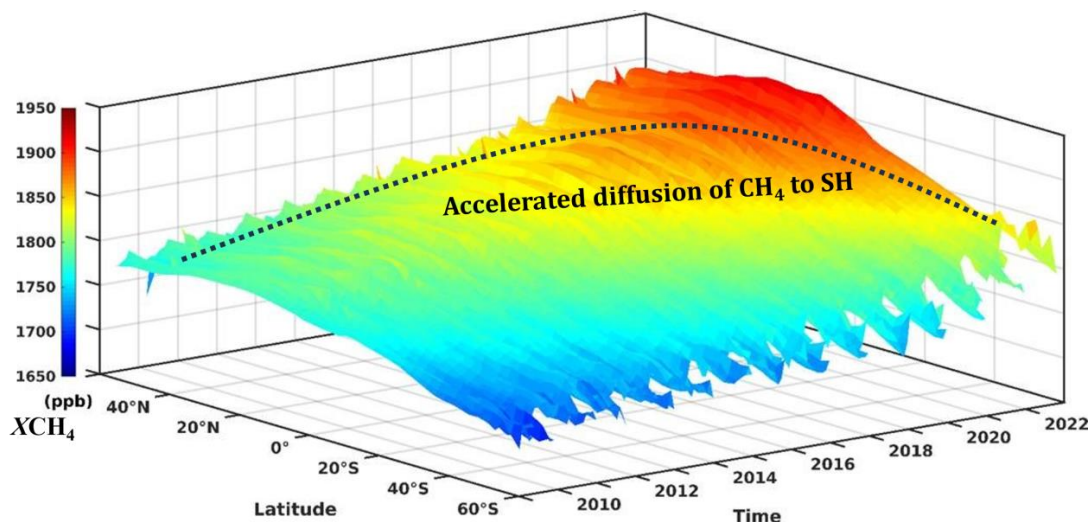
Figure 3 a) Remote Sensing (GOSAT) of atmospheric CH<sub>4</sub> variability over the Indian sub-continent b) ~~anomaly~~ Anomaly during 2009 to 2022 and c) identification of probable high CH<sub>4</sub> concentration using S5P/TROPOMI data from 2019 to 2022.

270 In the present study, we examined the annual space-time distribution of the XCH<sub>4</sub> obtained from the GOSAT-1 and GOSAT-2 over South Asia as shown in Figures 3a-b from 2009 to 2022

(N=14 years)—the long-term trends in  $XCH_4$  increased from 1700 ppb to 1950 ppb from 2009 to 2022 with an annual growth rate of  $8.76 \text{ ppb year}^{-1}$ . This growth rate is statistically tested with a p-value less than 0.05 for  $n=3803$  observations. A distinct, evident annual growth in  $CH_4$  is seen over the Indian subcontinent. Figure 3b shows the spatio-temporal residuals calculated using the data from 2009 to 2022. Residuals indicate that the acceleration of  $CH_4$  emissions in India has been significant since 2015. Before 2015, the  $CH_4$  concentrations were nearly uniformly distributed. To identify the critical potential high emission zones of  $CH_4$ , the present study applied the 90<sup>th</sup> percentile statistical filter, as shown in Figure 3c. The percentile is often used to detect the points that are significantly different from the rest of the data. Statistically significant high concentrations of  $CH_4$  are observed in tropical regions.

In the blue highlighted box, higher concentrations of  $CH_4$  were observed in the Indo-Gangetic Plain (IGP) and northwest (NW) areas of India, southeast of China, and NW of China. Southern China and north China are marked with wetlands and rice paddy fields, which are the primary sources of  $CH_4$  (Kavitha et al., 2018; [Chandra et al., 2019](#); [Guo et al., 2023](#)). High concentrations of  $CH_4$  over the IGP and NW are due to the population density and various industries that contribute to the emissions of  $CH_4$  and emissions from the rice paddy fields, respectively. In the present study, Figure 1 also shows the locations of coal and thermal power plants in India. Globally, the tropical wetlands ecosystem accounts for about 20% of the total global source (Saunois et al., 2020; Shaw et al., 2022), evidenced by bottom-up and top-down inventories. The study in the following sections assessed the  $CH_4$  growth rate associated with the source type over the Indian region.

Figure 4 shows the spatiotemporal distribution of  $XCH_4$  as a function of latitude, which depicts the annual variability at each latitude covering the northern and southern hemispheres (SH). There is a transparent latitudinal gradient in space. A strong diffusion of  $CH_4$  is observed from the northern hemisphere to SH during 2009 to 2022. During 2010, the  $XCH_4$  was distributed nearly constantly at all latitudes, indicating the stability of emissions from natural and anthropogenic sources. However, the gradient between the NH and SH has narrowed down with a growth rate of  $12 \text{ ppb year}^{-1}$  in 2022, reflecting the dominance of anthropogenic emissions over the tropics and unidentified leaks from the tropical wetlands and natural gas (Rocher-Ros et al., 2023).



305 | Figure 4. Spatiotemporal distribution of annual  $XCH_4$  as a function of latitude during 2009 to 2022.

More thoroughly, the characteristics of regional and global spatiotemporal variations are revealed by the continuous  $XCH_4$  data in space and time. As shown in Figure 4, the  $XCH_4$  displays a latitudinal gradient, and each latitudinal zone's growth tendencies are comparable.

310

#### 4.2. Assessment of $XCH_4$ over different source types in India

315 | Figures 5a-c shows the monthly time series of  $XCH_4$  over the specific sources of  $CH_4$  plotted ~~dotted~~ in the Indian region ~~from~~ during 2009 to ~~2022~~ 2020. Over the Indian sub-continent and south-east Asia, ~~during~~ October to November exhibits the highest amounts of  $CH_4$ , while March through June often sees the lowest (Sreenivas et al., 2016; Song et al., 2023), because of the enormous diversity in the climate zones of the Asian region. The seasonal cycle (peak and trough) of  $XCH_4$  is strongly associated with the vegetation during the active phase of cultivation and reduced photochemical reaction by the hydroxyl radicals, respectively.

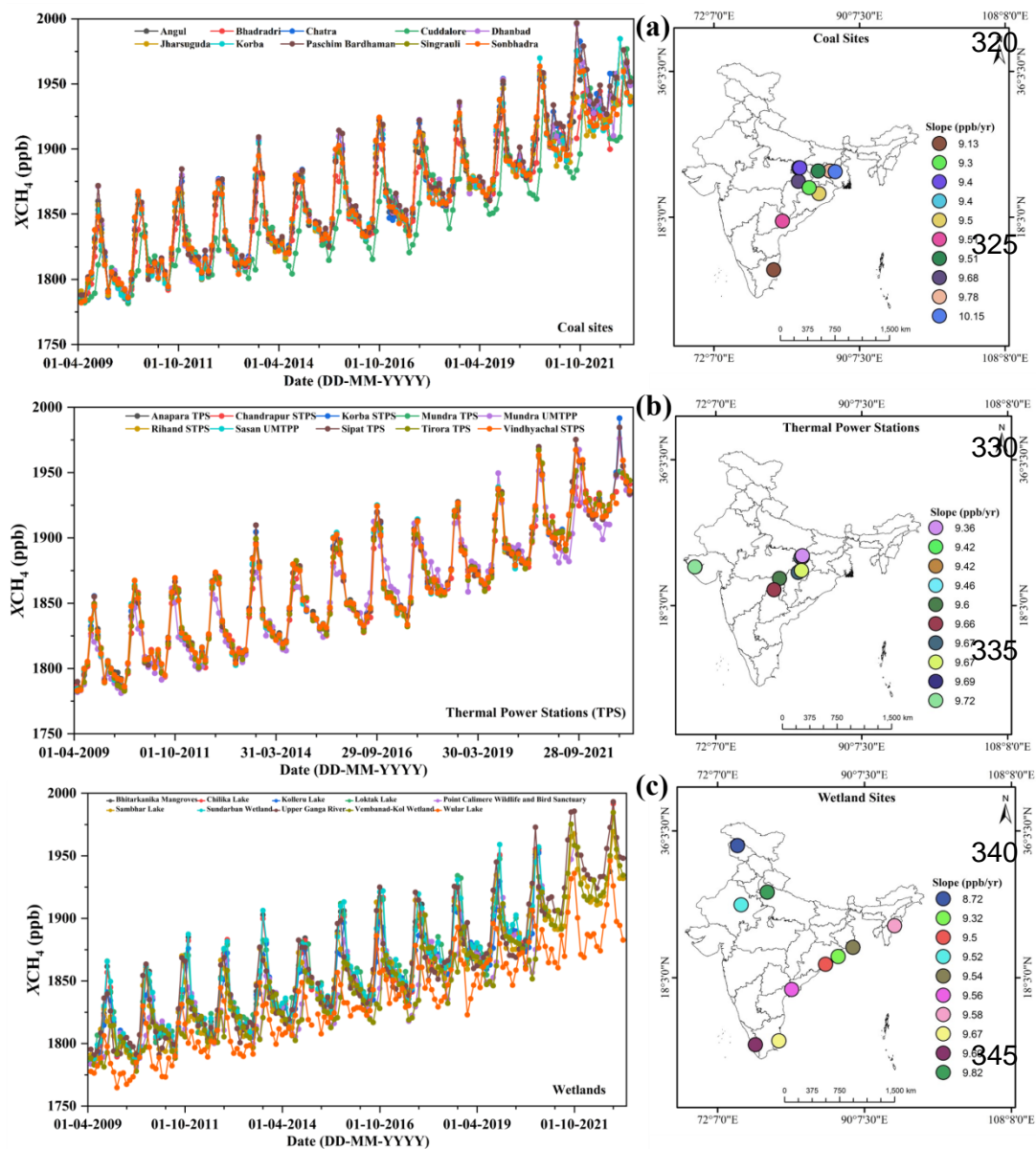


Figure 5. Monthly time series of  $XCH_4$  over the a)  $\mathbb{W}$ wetlands, b)  $\mathbb{T}$ hermal power stations, and c)  $\mathbb{C}$ oal fields: sources of emissions, along with the overall growth rate at the respective site.

350

Over the coal, thermal, and wetlands, the  $XCH_4$  shows typical seasonal behavior, with maximum activity during the post-monsoon (October-November) and minimum activity in the pre-monsoon (March-May), as shown in Figure 6. A seasonal maximum of  $XCH_4$  was observed over  $\mathbb{C}$ oal and  $\mathbb{T}$ hermal power plants from September to October and a minimum in pre-monsoon (March to May). In the case of wetlands, a shift in seasonal maxima varies from site to site, indicating their respective active phase of methanogens and the magnitude of the seasonal amplitude, which runs as a function of the individual wetland area. ~~A natural process known as methanogenesis causes wetlands to create  $CH_4$ .~~ Methanogens are microscopic organisms that break down organic substances in an oxygen-free environment. Thus, wetlands are perfect for

355

360 methanogens to grow and release  $\text{CH}_4$  since they are usually oxygen-poor, moist habitats (Zhang et al., 2023). Therefore, the present study investigated the above-listed wetlands. Most of the wetlands exhibit an annual growth rate of  $X\text{CH}_4$  greater than  $9.50 \text{ ppb year}^{-1}$  with high concentrations over Sundarbans wetland (Area = 423000 ha) exhibits a high concentration of  $\text{CH}_4$  with pronounced seasonality at all sites and lower concentrations over Wular Lake (area = 18900 ha) with an annual trend of  $8.72 \text{ ppb year}^{-1}$ .

365 During the examination period, the seasonal trends (slope) at each location, as summarised in Tables 1-3, were evaluated using Sen's slope-based Mann-Kendall test with a significance of p-value  $< 0.05$  (Pathakoti et al., 2021). The rate of increase in  $X\text{CH}_4$  was higher over the Upper Ganga (area = 26590 ha) with a slope of  $9.82 \text{ ppb year}^{-1}$  and followed by Vembanad-Kol Wetland (area = 151250 ha) with a slope of  $9.69 \text{ ppb year}^{-1}$ . Over the Sundarbans wetlands, West Bengal (area= 423000 ha) the rate of increase in  $X\text{CH}_4$  is  $9.54 \text{ ppb year}^{-1}$ . To investigate further, the present study quantified the source-based natural  $\text{CH}_4$  fluxes from each wetland using the WetCHARTs data in the following section.

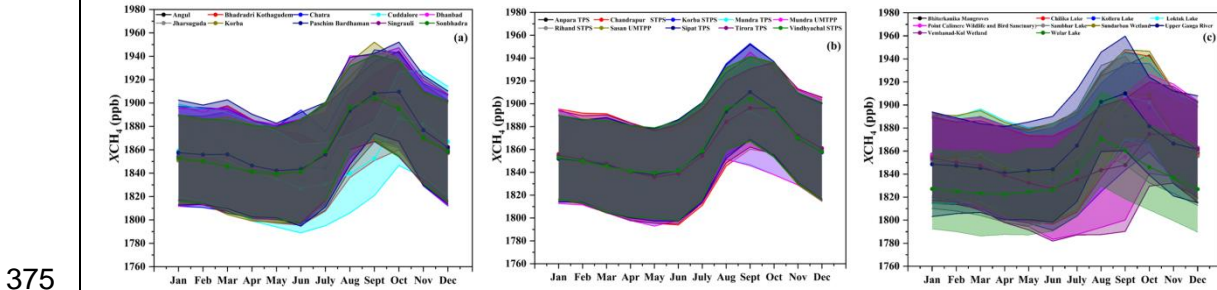
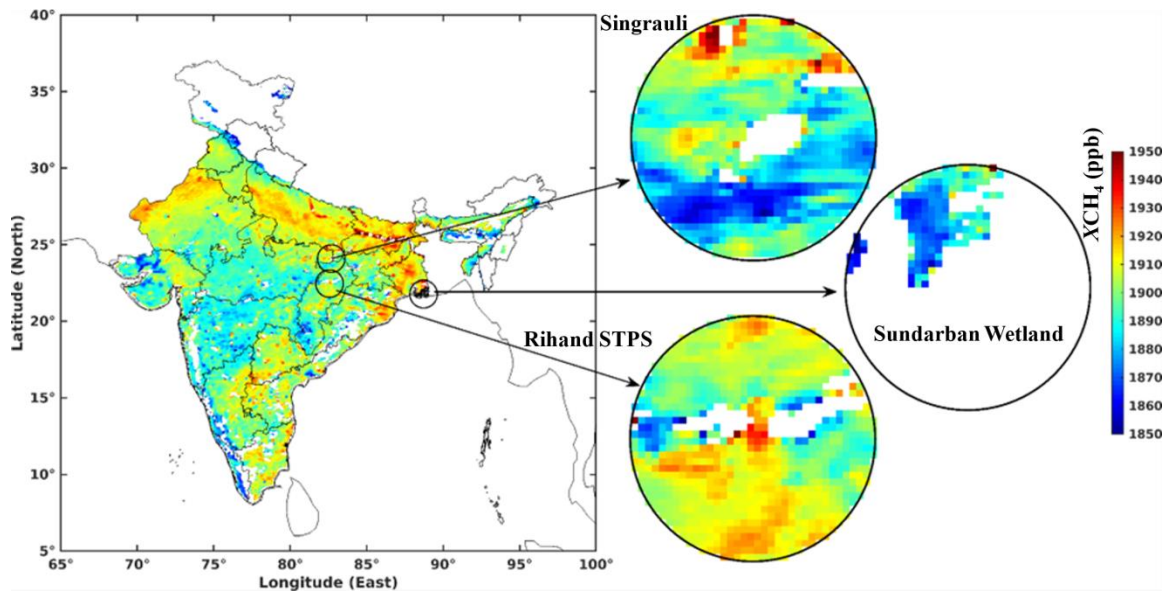


Figure 6. Seasonal  $X\text{CH}_4$  over a) coal fields, b) thermal power stations and c) wetlands.

380 The rate of increase in  $X\text{CH}_4$  was higher over the Sundarbans wetland, West Bengal, with a slope of  $8.61 \text{ ppb year}^{-1}$  and followed by the Loktak Lake (area=26600 ha), northeastern region (slope =  $8.60 \text{ ppb year}^{-1}$ ). The Vembanad-Kol wetland in Kerala is the country's second most extensive wetlands (area = 151250 ha). However, the rate of increase of  $X\text{CH}_4$  is slower (slope =  $7.73 \text{ ppb year}^{-1}$ ) among the top 10 wetlands. This study indicates that the Sundarbans and Loktak Lakes are rich in moist habitats that act as positive feedback to the leaks of  $\text{CH}_4$  into the atmosphere. An exciting phenomenon between the Loktak Lake and the Vembanad-Kol wetland was observed with an unexpectedly low growth rate of  $X\text{CH}_4$  over the Vembanad-Kol wetland. This phenomenon indicates that compared to other wetlands in India, the Vembanad-Kol wetland could reduce  $\text{CH}_4$  emissions through the methanotrophic process. Typically, the Indian climate is hot and humid, causing disturbances in the rainfall patterns; an increase in the waterlogged soils expands the wetlands (Zhang et al., 2023). Typical tropical wetlands are acting as positive feedback to climate change (Salimi et al., 2021).

390 Irrespective of the power production capacity, over the thermal power plants, the  $\text{CH}_4$  exhibited stabilized seasonality at each location. However the growth rate of  $X\text{CH}_4$  was higher over the

395 Mundra Ultra Mega power plant (UMPP), Gujarat with a slope of 9.72 ppb year<sup>-1</sup> followed by  
Mundra Thermal power station with a slope of 9.69 ppb year<sup>-1</sup>. The Mundra TPS and UMPP,  
Gujarat have a total power capacity of 8620MW with 14 units. With 2630 MW installed power  
capacity the Anpara TPS exhibited an XCH<sub>4</sub> growth rate of 9.36 ppb year<sup>-1</sup>. This indicated the  
higher potential power plants contribute more CH<sub>4</sub> emissions into the atmosphere. Over the coal  
400 mines, Paschim Bardhman (31.23 MT, 65mines) shows a high XCH<sub>4</sub> trend of about 10.15 ppb  
year<sup>-1</sup> followed by Dhanbad (31.25 MT, 51mines), Korba (120.47 MT, 15mines) which shows  
XCH<sub>4</sub> trend of 9.78 ppb year<sup>-1</sup> and 9.68 ppb year<sup>-1</sup> respectively. Angul (80.61MT, 13 mines) and  
Chatra (29.65 MT, 4 mines) show XCH<sub>4</sub> trend of 9.51 ppb year<sup>-1</sup>. The lowest annual trend in  
XCH<sub>4</sub> was observed over the Cuddalore coal mine (23.46 MT, 3 mines) which is about 9.13 ppb  
405 year<sup>-1</sup>. Anthropogenic emissions influence the methane growth trend is influenced by  
anthropogenic emissions. Wetland and biomass burning emissions determine the interannual  
variability (Fo et al., 2024). Figure 7 shows the continuous XCH<sub>4</sub> data from the  
S5P/TROPOMI at 0.05°×0.05°, complementing the GOSAT efforts in monitoring the XCH<sub>4</sub>  
dynamics in space and time. We demonstrated the spatiotemporal variation characteristics  
of XCH<sub>4</sub> more comprehensively at three different source type locations (Wetland, coal, and  
410 thermal power plant). High XCH<sub>4</sub> concentrations over the coal and thermal power station sites,  
and relatively lower concentrations in the wetland site. We concluded that the high-resolution  
S5P/TROPOMI has the potential to detect the point source variability. The growth rates  
of XCH<sub>4</sub> over the wetlands competes with coal sites with the production of over 30 MT, indicating an  
equivalent anthropogenic source. Results of the analysis in the context of thermal power plants  
415 and coal mines indicate that the emissions from the fossil fuels industries are significant, and the  
release of CH<sub>4</sub> into the atmosphere is commensurate with the production of the power and  
mining capacity.



420 Figure 7. S5P/TROPOMI XCH<sub>4</sub> gridded to 0.05° × 0.05° over Indian Region Indi and XCH<sub>4</sub>  
over wetland, coal, and thermal power plant sites with a radius of 100 km.

### 4.3 CH<sub>4</sub> fluxes from India's wetlands

In addition to the anthropogenic emissions, the present study utilised the global monthly wetlands emission fluxes from the Wetland Methane Emissions and Uncertainty (WetCHARTs v1.3.1) inventory (Bloom et al., 2017a, b). The figure 8 shows the monthly CH<sub>4</sub> fluxes over India's top 10 wetland sites from 2001 to 2019 and inset figure represents the long-term seasonally averaged CH<sub>4</sub> fluxes over wetlands. Emissions of CH<sub>4</sub> from the wetlands were minimal in the winter season (December to February) and pre-monsoon (March to May). In the tropical region, winter and pre-monsoon seasons are considered dry months with moderate to high temperatures and less precipitation. A study by Peng et al. (2022) and Feng et al. (2022) hypothesized that warmer and wetter wetlands contribute significantly to the high CH<sub>4</sub> emissions to the atmosphere. Typical climatological (1991-2020) mean temperature (accumulated seasonal precipitation) over India during winter, pre-monsoon, monsoon, and post-monsoon are 20 °C (23 mm), 28 °C (98 mm), 26 °C (867 mm) and 23°C (106 mm) respectively (<https://climateknowledgeportal.worldbank.org/country/india/climate-data-historical>). At all the wetland study sites during the study period, the maximum CH<sub>4</sub> flux was observed during the monsoon months with a maximum value of 23.62±3.66 mg m<sup>-2</sup> month<sup>-1</sup> over the Sundarbans wetland, which is the largest protected wetland of India and mangrove forest in the world. Besides climatic conditions, the emissions of CH<sub>4</sub> fluxes are positively correlated with the size of the wetland, thus observing maximum CH<sub>4</sub> flux over the Sundarbans site. High natural CH<sub>4</sub> emissions during the monsoon positively correlate with the atmospheric XCH<sub>4</sub> concentrations. Further, Mann-Kendall-based statistical analysis was carried out to assess the annual trend in the CH<sub>4</sub> emissions and found no significant trend over all the sites except Wular Lake, with an increasing rate of 0.04 mg m<sup>-2</sup> year<sup>-1</sup> with a p-value of 0.01. An annual trend of XCH<sub>4</sub> was over this study is about 8.73 ppb year<sup>-1</sup>. The current research highlights the need for further investigation to correlate in detail the temperature and associated precipitation influence on methane oxidation and microbial activities, thus modulating the CH<sub>4</sub> emissions from the wetlands.

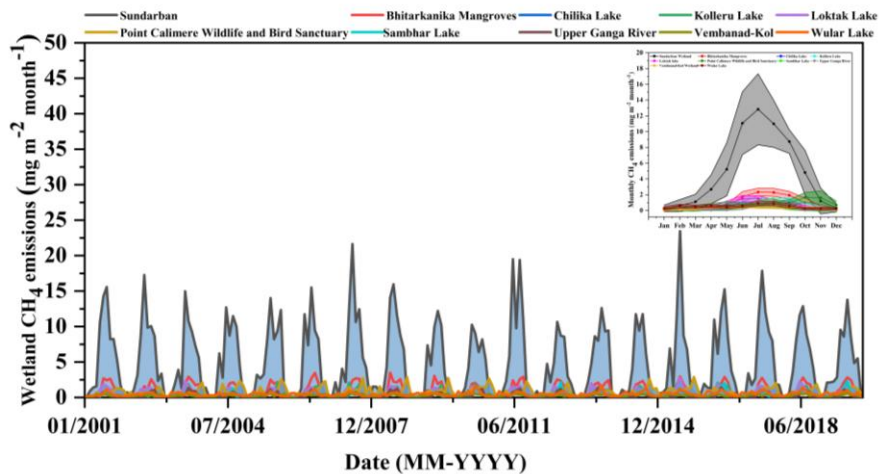
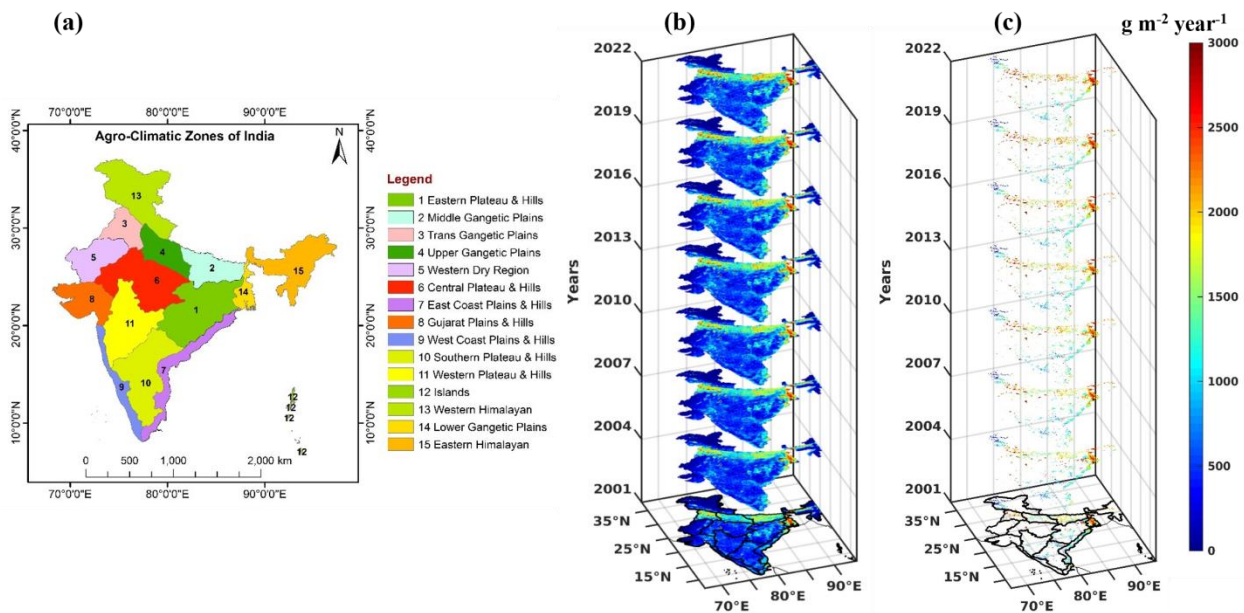


Figure 8: (a) Monthly Time series of Methane emissions (mg m<sup>-2</sup> month<sup>-1</sup>) over the wetland sites, inset figure shows the seasonal methane emissions over the wetland sites from 2001 to 2019.

#### 4.4 CH<sub>4</sub> emissions over India's Agroclimatic zones

India is divided into 15 agroclimatic zones according to the combination of soil types and climatic conditions (Choudhary and Sirohi, 2022). These zones offer a structure for the nation's development and execution of agricultural policies and practices. The crops and farming methods that are most appropriate for the environmental conditions in each zone are distinct from one another. Out of natural and anthropogenic sources of CH<sub>4</sub>, agricultural activity is also one of the dominant contributors to CH<sub>4</sub> dynamics in the atmosphere. Figures 9a-c8a-e show India's 15 agroclimatic zones and spatiotemporal trends of CH<sub>4</sub> emissions obtained from the bottom-up emission inventory of EDGAR (Crippa et al., 2020) from 2001 to 2022. Significant high emissions of CH<sub>4</sub>, as shown in Figure 9c8e7e, were observed over the Middle Gangetic Plains-MGP (2), Trans Gangetic Plains-TGP (3), Upper Gangetic Plains-UGP (4), East Coast Plains & Hills-ECPH (7), Lower Gangetic Plains-LGP (14) and East Gangetic Plains-EGP (15). These agroclimatic zones have active farming in rice, wheat, sugarcane, maize, millet, gram, cotton, etc. Besides traditional farming, the Lower Gangetic Plains has also actively contributed to livestock, horticulture, and forage production (Ahmad et al., 2017). Among all 15 agroclimatic zones, the MGP, TGP, UGP, ECPH, LGP and EGP have exhibited high emissions of CH<sub>4</sub> indicating the diversification of agricultural practices and homogenous traditions of agricultural production. Rice- wheat (R-W) based production system areis mainly being practiced in this region which is causing the negative effects on climate (Taneja et al., 2019). CH<sub>4</sub> emissions over the Northwest region areis exhibiting weak contribution compared to other agroclimatic zones of India.

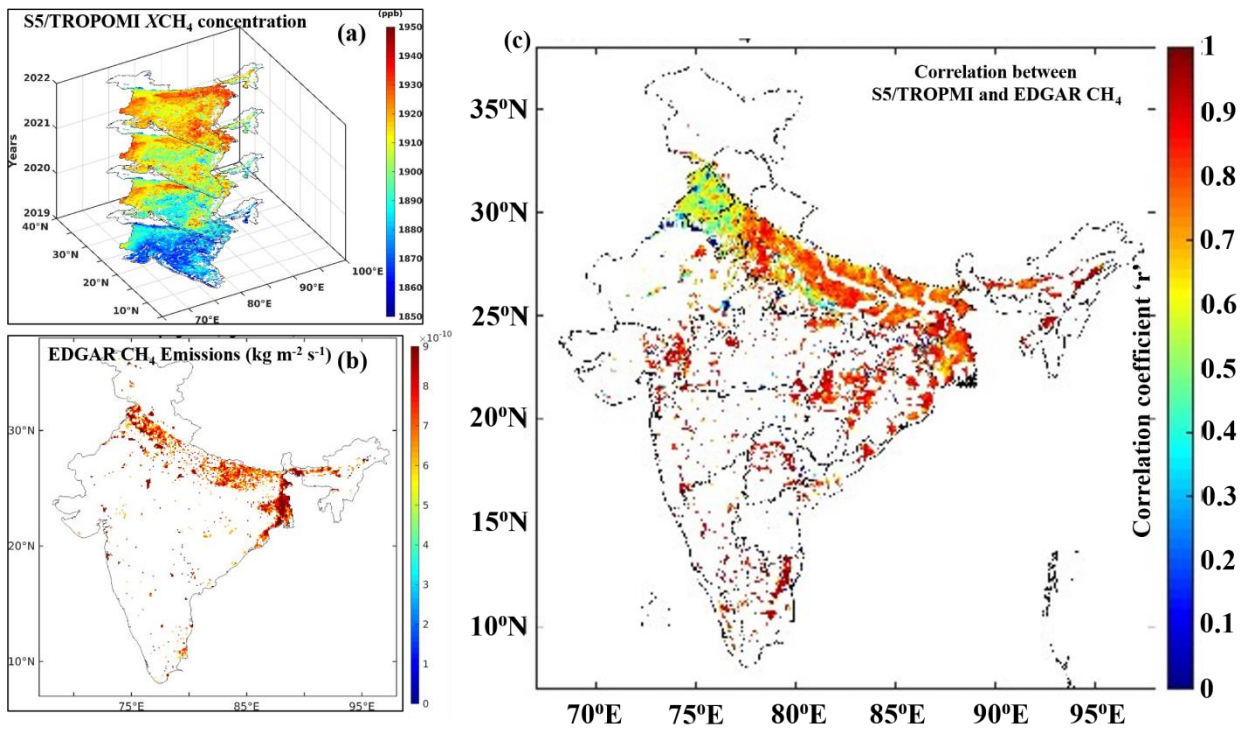


485 Figure 98. a) Agroclimatic zones of India, b) bottom-up CH<sub>4</sub> emissions inventory of EDGAR and c) 90<sup>th</sup> percentile statistical filter applied on CH<sub>4</sub> emissions from 2001 to 2022.



490 | **4.5. Spatial correlation between  $XCH_4$  concentrations and emissions over India**

To understand the relationship between India's high  $XCH_4$  concentration zones against emissions, we have computed pixel-level correlation between S5P/TROPOMI measured  $XCH_4$  concentrations and bottom-up inventory of EDGAR-based  $XCH_4$  anthropogenic emissions. Figures 910a-c shows  $XCH_4$  concentrations from S5P/TROPOMI, EDGAR-based anthropogenic emissions, and their correlation coefficient. The spatial patterns of  $XCH_4$  concentrations agree well with the high-emission regions. The correlation coefficient 'r' is strongly positive on in the IGP region, shows that more  $CH_4$  emission into the atmosphere through rapid industrial activity and anthropogenic contribution from human activity due to high population density. Besides the IGP region, the 'r' value is also strong in the east and northeast region due to the active anthropogenic emissions from natural sources such as agricultural activities, livestock, and wetlands (Behera et al., 2022).



505 | Figure 109. Pixel level correlation between S5P/TROPOMI based a)  $XCH_4$  concentrations and b) anthropogenic  $CH_4$  bottom-up emission inventory of EDGAR during 2019 to 2022 and c) correlation map.

510

## 5. Conclusion

515 Since the beginning of the Industrial Revolution, growing human populations have resulted in increased waste production, agriculture, and the use of fossil fuels. Therefore, this study demonstrated the spatiotemporal dynamics of  $XCH_4$  in the atmosphere and associated natural (wetlands) and anthropogenic sources (coal fields and thermal power plants) in the Indian region. The present study utilized the remote sensing based  $XCH_4$  data from the GOSAT and S5P/TROPOMI from 2009 to 2022. The following are the salient findings of the study.

- The present study demonstrated the continuous  $XCH_4$  data from the S5P/TROPOMI and GOSAT to effectively monitor the  $XCH_4$  dynamics in space and time.
- Long-term trends of  $XCH_4$  show significant annual growth from 2009 to 2022 in  $CH_4$  over the Indian subcontinent, with a yearly growth rate of 8.76 ppb which is in line with the global trend.
- Long-term temporal and spatial distribution characteristics and variations of  $CH_4$  emissions in India have accelerated in the last decade and globally, a substantial diffusion of  $CH_4$  is observed from the northern to southern hemisphere.
- $XCH_4$  levels peak in September-October over  $C_{coal}$  and  $T_{thermal}$  power plants but reach their minimum during March-May. The seasonal maxima of wetlands vary from site to site and are related to their size and active phase of methanogens.
- Majority of the wetlands show an annual growth rate in  $XCH_4$  is about 9.50 ppb year<sup>-1</sup>, indicates rich in moist habitats and active methanogens process.
- High  $XCH_4$  trend of 9.72 ppb year<sup>-1</sup> from the Mundra UMPP, Gujarat as well as the Paschim Bardhman coal mine (slope of 10.15 ppb year<sup>-1</sup>) indicated elevated and significant emissions from fossil fuels industries as compared to other natural sources.
- The highest  $CH_4$  flux was observed during the monsoon season over the Sundarbans wetland, the largest protected wetland in India, with a maximum value of 23.62±3.66 mg m<sup>-2</sup> month<sup>-1</sup>. Among the wetland sites, Wular Lake has a rising methane rate of 0.04 mg m<sup>-2</sup> month<sup>-1</sup> with a p-value of 0.01.
- The high levels of  $CH_4$  emissions seen in the MGP, TGP, UGP, ECPH, LGP, and EGP agroclimatic zones may be related to the varied farming methods and traditional agricultural output in these regions. Most of these areas revolve around the Rice–Wheat farming system which is negatively impacting the climate.
- The spatial patterns of  $XCH_4$  concentrations agree well with the high-emission regions. The correlation coefficient 'r' is strongly agreed in the IGP region.

545 Therefore we conclude that the space based  $XCH_4$  dataset provides significant support to track long-term changes in  $CH_4$  and provides insightful information on the causes and feedback mechanisms for the elevated concentrations of methane across the south Asia region.

550

## Code and data availability

555 GOSAT([https://data2.gosat.niesgo.jp/GosatDataArchive\\_Service/Usr/](https://data2.gosat.niesgo.jp/GosatDataArchive_Service/Usr/)),—TROPOMI ([https://disc.gsfc.nasa.gov/datasets/S5P\\_L2\\_CH4\\_HiR\\_2](https://disc.gsfc.nasa.gov/datasets/S5P_L2_CH4_HiR_2)) satellite data, EDGAR bottom up inventory(<https://edgar.jrc.ec.europa.eu/gallery?release=v50&substance=CH4&sector=TOTALS>) and wetland methane emissions and uncertainty ([https://daac.ornl.gov/CMS/guides/MonthlyWetland\\_CH4\\_WetCHARTs.html](https://daac.ornl.gov/CMS/guides/MonthlyWetland_CH4_WetCHARTs.html)) data used in the present study are freely available and can be downloaded as summarised in figure 2 with the user’s credentials. The code will be available from the author upon request.

## Declaration of Interest Statement

560 Authors declare no conflict of interest.

## Author Contribution

565 D.V. Mahalakshmi: [Conceptualization](#), Formal analysis, Writing – original draft. Mahesh P: Conceptualization, Formal analysis, Writing – original draft. A.L.Kanchana: [Conceptualization](#), Formal analysis, Writing – original draft. Sujatha. P: Formal data analysis, Writing – original draft. Ibrahim Shaik: Analysis. K.S. Rajan: Writing-review and Editing. Vijay Kumar Sagar: Formal Analysis and data curation. P. Raja: Writing-review and Editing. Y.K.Tiwari: Writing reviewing and Editing. Prakash Chauhan: Writing-review and Editing.

570

## Acknowledgement

We sincerely thank the Director, NRSC/ISRO, for his kind guidance and support. Authors greatly acknowledge the JAXA and National Institute of Environmental Studies (NIES) for providing free access to the GOSAT XCH<sub>4</sub> observations ([https://data2.gosat.niesgo.jp/GosatDataArchive\\_Service/usr/](https://data2.gosat.niesgo.jp/GosatDataArchive_Service/usr/) download accessed on 15 June 2023) and the Earthdata for giving access to the S5P/TROPOMI ([https://disc.gsfc.nasa.gov/datasets/S5P\\_L2\\_CH4\\_HiR\\_2/summary](https://disc.gsfc.nasa.gov/datasets/S5P_L2_CH4_HiR_2/summary) accessed on 15 June 2023) data. We also thank the European Commission’s Joint Research Centre (JRC) for providing the CH<sub>4</sub> bottom-up inventory of EDGAR (<https://edgar.jrc.ec.europa.eu/gallery?release=v50&substance=CH4&sector=TOTALS>, accessed on 25 July 2023). [The authors also thank the Oak Ridge National Laboratory \(ORNL\) Distributed Active Archive Center \(DAAC\) for providing the wetland methane emissions data.](#) This work has been carried out as part of [Technology Development Project \(TDP\)](#) titled “Investigation of Atmospheric GHGs Emissions over the Indian Region (AGE)” and the Land- Ocean-Atmospheric GHGs Interaction Experiments (LOAGIN-X) of Climate and Atmospheric Processes of [ISRO-Geopshere Biosphere P programme \(CAP-IGBP\)](#). [We are very grateful to the anonymous reviewers and the handling editor for their constructive comments and suggestions, which have helped us to improve the manuscript.](#)

585

## References

- 590 [Ahmad, L., Habib Kanth, R., Parvaze, S., Sheraz Mahdi, S., Ahmad, L., Habib Kanth, R., Parvaze, S. and Sheraz Mahdi, S.: Agro-climatic and agro-ecological zones of India, 99-118 2017.](#)
- 595 [Balcombe, P., Speirs, J. F. , Brandon, N. P. , & Hawkes, A. D.: Methane emissions: Choosing the right climate metric and time horizon, \*Environmental Science: Processes and Impacts\*, 20\(10\), 1323–1339, 10.1039/C8EM00414E, 2018.](#)
- 600 [Bassi, N., Dinesh, K.M., Anuradha, S., and PardhaSaradhi, P.: Status of wetlands in India: A review of extent, ecosystem benefits, threats and management strategies, \*J. Hydrol. Reg. Stud\* 2, 1, 2014.](#)
- 605 [Behera, M.D., Mudi, S., Shome, P., Das, P.K., Kumar, S., Joshi, A., Rathore, A., Deep, A., Kumar, A., Sanwariya, C. and Kumar, N.: COVID-19 slowdown induced improvement in air quality in India: Rapid assessment using Sentinel-5P TROPOMI data, \*Geocarto International\*, 37\(25\), 8127-8147. <https://doi.org/10.1080/10106049.2021.1993351>, 2022.](#)
- 610 [Bergamaschi, P., Segers, A., Brunner, D., Haussaire, J.M., Henne, S., Ramonet, M., Arnold, T., Biermann, T., Chen, H., Conil, S. and Delmotte, M.: High-resolution inverse modelling of European CH<sub>4</sub> emissions using the novel FLEXPART-COSMO TM5 4DVAR inverse modelling system, \*Atmospheric Chemistry and Physics\*, 22\(20\), pp.13243-13268, 2022.](#)
- 615 [Bloom, A. A., K. Bowman, M. Lee, A. J. Turner, R. Schroeder, J. R. Worden, R. J. Weidner, K. C. McDonald, and D. J. Jacob.: CMS: Global 0.5-deg Wetland Methane Emissions and Uncertainty \(WetCHARTs v1.0\), \*ORNL DAAC\*, Oak Ridge, Tennessee, USA, <https://doi.org/10.3334/ORNLDAAC/1502>, 2017b.](#)
- 620 [Bloom, A. A., K. W. Bowman, M. Lee, A. J. Turner, R. Schroeder, J. R. Worden, R. Weidner, K. C. McDonald, and D. J. Jacob.: A global wetland methane emissions and uncertainty dataset for atmospheric chemical transport models \(WetCHARTs version 1.0\), \*Geosci. Model Dev.\*, 10, 2141–2156, <https://doi.org/10.5194/gmd-10-2141-2017>, 2017a.](#)
- 625 [Bloom, A.A., K.W. Bowman, M. Lee, A.J. Turner, R. Schroeder, J.R. Worden, R.J. Weidner, K.C. McDonald, and D.J. Jacob.: CMS: Global 0.5-deg Wetland Methane Emissions and Uncertainty \(WetCHARTs v1.3.1\), ORNL DAAC, Oak Ridge, Tennessee, USA, <https://doi.org/10.3334/ORNLDAAC/1915>, 2021.](#)

Chandra, N., Hayashida, S., Saeki, T., & Patra, P. K.: What controls the seasonal cycle of columnar methane observed by GOSAT over different regions in India?, *Atmospheric Chemistry and Physics*, 17(20), 12633-12643. <https://doi.org/10.5194/acp-17-12633-2017>, 2017.

630 [Choudhary, B.B., Sirohi, S.: Understanding vulnerability of agricultural production system to climatic stressors in North Indian Plains: a meso-analysis, \*Environ Dev Sustain\*, 24, 13522–13541, <https://doi.org/10.1007/s10668-021-01997-7>, 2022.](https://doi.org/10.1007/s10668-021-01997-7)

635 [Crippa, M., Solazzo, E., Huang, G., Guizzardi, D., Koffi, E., Muntean, M., Schieberle, C., Friedrich, R. and Janssens-Maenhout, G.: High resolution temporal profiles in the Emissions Database for Global Atmospheric Research, \*Scientific data\*, 7\(1\), p.121, 2020.](https://doi.org/10.1038/s41598-020-12111-1)

640 [Feng, L., Palmer, P.I., Zhu, S., Parker, R.J. and Liu, Y.: Tropical methane emissions explain large fraction of recent changes in global atmospheric methane growth rate, \*Nature communications\*, 13\(1\), p.1378, 2022.](https://doi.org/10.1038/s41467-022-28111-1)

645 [Frankenberg, C., Aben, I. P. B. J. D. E., Bergamaschi, P., Dlugokencky, E. J., Van Hees, R., Houweling, S., P. Van Der Meer, R. Snel, & Tol, P.: Global column-averaged methane mixing ratios from 2003 to 2009 as derived from SCIAMACHY: Trends and variability, \*Journal of Geophysical Research: Atmospheres\*, 116\(D4\), <https://doi.org/10.1029/2010JD014849>, 2011.](https://doi.org/10.1029/2010JD014849)

650 [Fu, B., Jiang, Y., Chen, G., Lu, M., Lai, Y., Suo, X., & Li, B.: Unraveling the dynamics of atmospheric methane: the impact of anthropogenic and natural emissions, \*Environmental Research Letters\*, 2024.](https://doi.org/10.1029/2024GL071111)

655 [Ganesan, A. L., Schwietzke, S., Poulter, B., Arnold, T., Lan, X., Rigby, M., Vogel, F. R., van der Werf, G. R., Janssens-Maenhout, G., Boesch, H., Pandey, S., Manning, A. J., Jackson, R. B., Nisbet, E. G., and Manning, M. R.: Advancing scientific understanding of the global methane budget in support of the Paris Agreement, \*Global Biogeochem. Cy.\*, 33, 1475–1512, <https://doi.org/10.1029/2018GB006065>, 2019.](https://doi.org/10.1029/2018GB006065)

660 [Goroshi, S. K., Singh, R. P., Panigrahy, S., & Parihar, J. S.: Analysis of seasonal variability of vegetation and methane concentration over India using SPOT-VEGETATION and ENVISAT-SCIAMACHY data, \*Journal of the Indian Society of Remote Sensing\*, 39, 315-321, 2011.](https://doi.org/10.1080/01431161.2011.601111)

665 [Goroshi, S. K., Singh, R. P., Panigrahy, S., and Parihar, J. S.: Analysis of seasonal variability of vegetation and methane concentration over India using SPOT-VEGETATION and ENVISATSCIAMACHY data, \*J. Indian Soc. Remote Sens.\*, 39, 315–321, <https://doi.org/10.1007/s12524-011-0097-z>, 2011.](https://doi.org/10.1007/s12524-011-0097-z)

670 Hayashida, S., Ono, A., Yoshizaki, S., Frankenberg, C., Takeuchi, W., and Yan, X.: Methane concentrations over Monsoon Asia as observed by SCIAMACHY: signals of methane emission from rice cultivation, Remote Sens. Environ., 139, 246–256, <https://doi.org/10.1016/j.rse.2013.08.008>, 2013.

675 Huang, L., Tang, M., Fan, M., & Cheng, H.: Density functional theory study on the reaction between hematite and methane during chemical looping process, Applied Energy, 159, 132-144, 2015.

IPCC: Climate change.: The physical science basis, Contribution of Working Group I to the sixth assessment report of the intergovernmental panel on climate change, 2021.

680 Kang, M., Mauzerall, D. L., Ma, D. Z., & Celia, M. A.: Reducing methane emissions from abandoned oil and gas wells: Strategies and costs. Energy Policy, 132, 594-601, 2019.

Kavitha, M., & Nair, P. R.: Region-dependent seasonal pattern of methane over Indian region as observed by SCIAMACHY, Atmospheric environment, 131, 316-325, 2016.

685 Kavitha, M., Nair, P. R., Girach, I. A., Aneesh, S., Sijikumar, S., & Renju, R.: Diurnal and seasonal variations in surface methane at a tropical coastal station, Role of mesoscale meteorology, Science of the total environment, 631, 1472-1485, 2018.

690 Kirschke, S., Bousquet, P., Ciais, P., Saunio, M., Canadell, J. G., Dlugokencky, E. J., Bergamaschi, P., Bergmann, D., Blake, D. R., Bruhwiler, L., Cameron-Smith, P., Castaldi, S., Chevallier, F., Feng, L., Fraser, A., Heimann, M., Hodson, E. L., Houweling, S., Josse, B., Fraser, P. J., Krummel, P. B., Lamarque, J.- F., Langenfelds, R. L., Quéré, C. L., Naik, V., O’Doherty, S., Palmer, P. I., Pison, I., Plummer, D., Poulter, B., Prinn, R. G., Rigby, M., Ringeval, B., Santini, M., Schmidt, M., Shindell, D. T., Simpson, I. J., Spahni, R., Steele, L. P., Strode, S. A., Sudo, K., Szopa, S., Werf, G. R. van der, Voulgarakis, A., Weele, M. van, Weiss, R. F., Williams, J. E., and Zeng, G.: Three decades of global methane sources and sinks, Nat. Geosci., 6, 1–11, <https://doi.org/10.1038/ngeo1955>, 2013.

695 Kozicka, K., Orazalina, Z., Gozdowski, D., & Wójcik-Gront, E.: Evaluation of temporal changes in methane content in the atmosphere for areas with a very high rice concentration based on Sentinel-5P data, Remote Sensing Applications, Society and Environment, 30, 100972, <https://doi.org/10.1016/j.rsase.2023.100972>, 2023.

700 Kuze, A., Suto, H., Nakajima, M. and Hamazaki, T.: Thermal and near infrared sensor for carbon observation Fourier-transform spectrometer on the Greenhouse Gases Observing Satellite for greenhouse gases monitoring. Applied optics, 48(35), pp.6716-6733, 2009..

705

710 Lan, X., K.W. Thoning, and E.J. Dlugokencky.: Trends in globally-averaged CH<sub>4</sub>, N<sub>2</sub>O, and SF<sub>6</sub> determined from NOAA Global Monitoring Laboratory measurements, Version 2024-01, <https://doi.org/10.15138/P8XG-AA10>

715 Nair, P. R., & Kavitha, M.: Stratospheric distribution of methane over a tropical region as observed by MIPAS on board ENVISAT, International Journal of Remote Sensing, 41(21), 8380-8405, 2020.

720 Parker, R. J., Boesch, H., McNorton, J., Comyn-Platt, E., Gloor, M., Wilson, C., ... & Bloom, A. A.: Evaluating year-to-year anomalies in tropical wetland methane emissions using satellite CH<sub>4</sub> observations. Remote Sensing of Environment, 211, 261-275. <https://doi.org/10.1016/j.rse.2018.02.011>, 2018.

725 Pathakoti, M., Santhoshi, T., Aarathi, M., Mahalakshmi, D.V., Kanchana, A.L., Srinivasulu, J., SS, R.S., Soni, V.K., MVR, S.S. and Raja, P.: Assessment of spatio-temporal climatological trends of ozone over the Indian region using machine learning, Spatial Statistics, 43, p.100513. [10.1016/j.spasta.2021.100513](https://doi.org/10.1016/j.spasta.2021.100513), 2021.

730 Peng, S., Lin, X., Thompson, R.L., Xi, Y., Liu, G., Hauglustaine, D., Lan, X., Poulter, B., Ramonet, M., Saunois, M. and Yin, Y.: Wetland emission and atmospheric sink changes explain methane growth in 2020. Nature, 612(7940), pp.477-482, 2022.

735 Rocher-Ros, G., Stanley, E.H., Loken, L.C., Casson, N.J., Raymond, P.A., Liu, S., Amatulli, G. and Sponseller, R.A.: Global methane emissions from rivers and streams, Nature, 621(7979), pp.530-535, <https://doi.org/10.1038/s41586-023-06344-6>, 2023.

740 S. Pai and H. Zerriffi, "A novel dataset for analysing sub-national socioeconomic developments in the Indian coal industry," IOP SciNotes, vol. 2, no. 1, p. 014001, Mar. 2021, doi: 10.1088/2633-1357/abdbbb.

745 S. Salimi., S.A.A.A.N. Almuktar and M. Scholz.: Impact of climate change on wetland ecosystems: A critical review of experimental wetlands, Journal of Environmental Management, <https://doi.org/10.1016/j.jenvman.2021.112160>, 2021.

Sagar, V. K., Pathakoti, M., Mahalakshmi, D. V., Rajan, K. S., MVR, S. S., Hase, F., ... & Sha, M. K.: Ground-Based Remote Sensing of Total Columnar CO<sub>2</sub>, CH<sub>4</sub>, and CO Using EM27/SUN FTIR Spectrometer at a Suburban Location (Shadnagar) in India and Validation of Sentinel-5P/TROPOMI, IEEE Geoscience and Remote Sensing Letters, 19, 1-5. [10.1109/LGRS.2022.3171216](https://doi.org/10.1109/LGRS.2022.3171216), 2022.

- 750 Sakalli, A., Cescatti, A., Dosio, A., & Gücel, M. U.: Impacts of 2 C global warming on primary production and soil carbon storage capacity at pan-European level, *Climate Services*, 7, 64-77, 2017.
- Saunio M et al 2016a The global methane budget 2000-2012 *Earth Syst. Sci. Data* 8 697–751. <https://doi.org/10.5194/essd-8-697>, 2016.
- 755 Schaefer, H., Fletcher, S. E. M., Veidt, C., Lassey, K. R., Brailsford, G. W., Bromley, T. M., Dlugokencky, E. J., Michel, S. E., Miller, J. B., Levin, I., Lowe, D. C., Martin, R. J., Vaughn, B. H., and White, J. W. C.: A 21st century shift from fossil-fuel to biogenic methane emissions indicated by 13CH<sub>4</sub>, *Science*, 352, <https://doi.org/10.1126/science.aad2705>, 2016.
- 760 Schneising, O., Buchwitz, M., Burrows, J. P., Bovensmann, H., Bergamaschi, P., and Peters, W.: Three years of greenhouse gas column-averaged dry air mole fractions retrieved from satellite – Part 2: Methane, *Atmos. Chem. Phys* 9, 443–465, doi:10.5194/acp-9-443-2009, 2009.
- 765 Shaw, Jacob T., et al. "Large Methane Emission Fluxes Observed from Tropical Wetlands in Zambia.: <https://doi.org/10.1029/2021GB007261>, 2022.
- Song, H., Sheng, M., Lei, L., Guo, K., Zhang, S. and Ji, Z.: Spatial and Temporal Variations of Atmospheric CH<sub>4</sub> in Monsoon Asia Detected by Satellite Observations of GOSAT and TROPOMI. *Remote Sensing*, 15(13), p.3389, <https://doi.org/10.3390/rs15133389>, 2023.
- 770 Sreenivas, G., Mahesh, P., Subin, J., Kanchana, A. L., Rao, P. V. N., &Dadhwal, V. K.: Influence of meteorology and interrelationship with greenhouse gases (CO<sub>2</sub> and CH<sub>4</sub>) at a suburban site of India, *Atmospheric Chemistry and Physics*, 16, 3953-3967,doi.org/10.5194/acp-16-3953-2016, 2016.
- 775 Sreenivas, G., P. Mahesh, D. V. Mahalakshmi, A. L. Kanchana, Naveen Chandra, Prabir K. Patra, P. Raja, Shesha Sai MVR, Sripada S, Rao PV, Dadhwal VK.: Seasonal and annual variations of CO<sub>2</sub> and CH<sub>4</sub> at Shadnagar, a semi-urban site, *Science of The Total Environment*, 819:153114, <https://doi.org/10.1016/j.scitotenv.2022.153114>, 2022.
- 780 Taneja, G., Pal, B.D., Joshi, P.K., Aggarwal, P.K. and Tyagi, N.K.: Farmers’ preferences for climate-smart agriculture—an assessment in the Indo-Gangetic Plain (pp. 91-111). Springer Singapore, 2019 .
- 785



- Turner, A. J., Frankenberg, C., and Kort, E. A.: Interpreting contemporary trends in atmospheric methane, *P. Natl. Acad. Sci. USA*, 116, 2805–2813, <https://doi.org/10.1073/pnas.1814297116>, 2019
- 790 Vinna°, L., Medhaug, I., and Schmid, M. (2021). The vulnerability of lakes to climate change along an altitudinal gradient. *Commun. Earth Environ.* 2, 35. <https://doi.org/10.1038/s43247-021-00106-w>
- 795 Wang, Y., Yang, H., Ye, C., Chen, X., Xie, B., Huang, C., Zhang, J. and Xu, Mx.: Effects of plant species on soil microbial processes and CH<sub>4</sub> emission from constructed wetlands. *Environmental pollution*, 174, pp.273-278, 2013.
- Wang, Y., Yang, H., Ye, C., Chen, X., Xie, B., Huang, C., Zhang, J. and Xu, M.: Effects of plant species on soil microbial processes and CH<sub>4</sub> emission from constructed wetlands. *Environmental pollution*, 174, pp.273-278, 2013.
- 800 Worden, J. R., Bloom, A. A., Pandey, S., Jiang, Z., Worden, H. M., Walker, T. W., Houweling, S., and Röckmann, T.: Reduced biomass burning emissions reconcile conflicting estimates of the post-2006 atmospheric methane budget, *Nat. Commun.*, 8, 1–11, <https://doi.org/10.1038/s41467-017-02246-0>, 2017.
- 805 Zhang, L., Tian, H., Shi, H., Pan, S., Chang, J., Dangal, S. R., ... & Jackson, R. B.: A 130-year global inventory of methane emissions from livestock: Trends, patterns, and drivers. *Global Change Biology*, 28(17), 5142-5158, <https://doi.org/10.1111/gcb.16280>, 2022.
- 810 Zhang, Z., Poulter, B., Feldman, A.F., Ying, Q., Ciais, P., Peng, S. and Li, X.: Recent intensification of wetland methane feedback. *Nature Climate Change*, 13(5), pp.430-433. <https://doi.org/10.1038/s41558-023-01629-0>, 2023.